PNAS RESEARCH ARTICLE | CELL BIOLOGY

Cytoplasmic fluidization contributes to breaking spore dormancy in fission yeast

Keiichiro Sakai[a,b,1], Yohei Kondo[a,b,c,d,e,1], Yuhei Goto[a,b,c,d,e,2], and Kazuhiro Aoki[a,b,c,d,e,2]

Affiliations are included on p. 9.

Edited by John Pringle, Stanford University School of Medicine, Stanford, CA; received April 2, 2024; accepted May 9, 2024

The cytoplasm is a complex, crowded environment that influences myriad cellular processes including protein folding and metabolic reactions. Recent studies have suggested that changes in the biophysical properties of the cytoplasm play a key role in cellular homeostasis and adaptation. However, it still remains unclear how cells control their cytoplasmic properties in response to environmental cues. Here, we used fission yeast spores as a model system of dormant cells to elucidate the mechanisms underlying regulation of the cytoplasmic properties. By tracking fluorescent tracer particles, we found that particle mobility decreased in spores compared to vegetative cells and rapidly increased at the onset of dormancy breaking upon glucose addition. This cytoplasmic fluidization depended on glucose-sensing via the cyclic adenosine monophosphate-protein kinase A pathway. PKA activation led to trehalose degradation through trehalase Ntp1, thereby increasing particle mobility as the amount of trehalose decreased. In contrast, the rapid cytoplasmic fluidization did not require de novo protein synthesis, cytoskeletal dynamics, or cell volume increase. Furthermore, the measurement of diffusion coefficients with tracer particles of different sizes suggests that the spore cytoplasm impedes the movement of larger protein complexes (40 to 150 nm) such as ribosomes, while allowing free diffusion of smaller molecules (~3 nm) such as second messengers and signaling proteins. Our experiments have thus uncovered a series of signaling events that enable cells to quickly fluidize the cytoplasm at the onset of dormancy breaking.

fission yeast | germination | cytoplasmic fluidity | cAMP-PKA pathway | trehalose

Significance

Cellular processes are influenced by the biophysical properties of the cytoplasm such as crowding and viscoelasticity. Although it has been suggested that cells tune the cytoplasmic properties in response to environmental changes, the molecular mechanisms remain unclear. Here, we used the dormant fission yeast spores and uncovered signaling pathways that facilitate cytoplasmic fluidization during dormancy breaking. Furthermore, we tracked the mobility of intracellular tracer particles and found that the spore cytoplasm impedes the mobility of larger protein complexes, while allowing free diffusion of smaller molecules. These results suggest that small signaling proteins can diffuse relatively freely in the spore cytoplasm and have the ability to transmit dormancy-breaking signals, while the motion of large complexes, such as ribosomes, is restricted.

The cytoplasm is a crowded environment that is densely packed with macromolecules (e.g., proteins, nucleic acids, lipids) and organelles. The crowded environments decrease the mobility of molecules and inhibit diffusion-limited reactions by reducing the encounter rates of molecules; on the other hand, the crowded conditions can also promote intermolecular assembly through entropic effects and facilitate reaction-limited reactions. Furthermore, accumulating evidence has shown that the cytoplasm is not a simple crowded milieu, but rather displays a complex porous structure (1–3), which is not reproduced by in vitro assays such as Bovine Serum Albumin (BSA) solution (4, 5). In addition, there is rapidly growing interest in the physiological significance of cytoplasmic viscoelasticity and pH (6, 7). The cytoplasmic structures and physico-chemistry influence many different biochemical reactions and cellular organization (8, 9), including microtubule dynamics (10), protein production (11), phase separation (12), and kinase reactions (13–15).

The biophysical properties, such as the structures and physico-chemistry, of the cytoplasm are disturbed by environmental changes. For example, hyperosmotic stress enhances molecular crowding through dehydration, which inhibits macromolecular movement (10, 12, 16, 17). Energy depletion and nutrient starvation also cause reduced motion of macromolecules in the cytoplasm (7, 18–21). However, to adapt to environmental changes, cells maintain homeostasis by autonomously regulating the biophysical properties of the cytoplasm. A recent study has shown that mammalian cells possess a molecular crowding sensor, WNK1, which leads to cell volume recovery and reduced crowding in response to hyperosmotic stress (22). As another example, upon temperature increase, budding yeast cells synthesize trehalose and glycogen to increase cytoplasmic viscosity, which counteracts the increase in protein diffusivity (23).

Dormancy is a cellular state, in which the metabolic activity is decreased and the cell cycle is reversibly arrested under unfavorable conditions (7, 24). Those characteristics link to the cytoplasmic properties of dormant cells with reduced fluidity and molecular mobility. For example, it is known that the cytoplasms of dormant cells show solid or glass-like properties due to their reduced water content; such characteristic cytoplasms are observed in diverse species such as bacterial spores (25, 26), fungal spores (27), plant seeds (28), tardigrades (29),

The authors declare no competing interest.

This article is a PNAS Direct Submission.

[1]K.S. and Y.K. contributed equally to this work.

[2]To whom correspondence may be addressed. Email: goto.yuhei.4c@kyoto-u.ac.jp or aoki.kazuhiro.6v@kyoto-u.ac.jp.

This article contains supporting information online at https://www.pnas.org/lookup/suppl/doi:10.1073/pnas.2405553121/-/DCSupplemental.

Published June 18, 2024.

and sleeping chironomids (30). Recently, microrheological measurements revealed that macromolecular mobility is restricted inside the cytoplasm of dormant cells (7, 19, 24). However, it remains unclear what molecular mechanisms are involved in the reversible change in cytoplasmic fluidity and which and how intracellular signaling pathways govern these processes. In particular, since the cytoplasmic properties in a dormant state suppress intracellular diffusion and reaction, it is puzzling how dormant cells can still achieve a rapid resumption of cell growth when environmental conditions improve.

Here, we demonstrate that the glucose-sensing pathway triggers cytoplasmic fluidization during dormancy breaking of spores in the fission yeast *Schizosaccharomyces pombe*. The fission yeast enters a dormant state by forming spores under nutrient starvation, and glucose refeeding breaks the dormancy, which is called germination. By using microrheological tracer particles, we show that the cytoplasmic fluidity of spores is limited compared to that of vegetative cells. The solidified cytoplasm in spores rapidly fluidizes upon glucose stimulation. This fluidization process is dependent on the degradation of trehalose, which is regulated by the cAMP-PKA (cyclic adenosine monophosphate-protein kinase A) pathway. Based on our findings using tracer particles of different sizes, we propose the existence of a dormancy-specific intracellular milieu, which impedes diffusion of large protein complexes such as ribosomes, while allowing relatively free diffusion of small signaling proteins.

Results

Fission Yeast Spores Restrict the Movement of Particles with a Diameter of 40 nm. In this study, we adopted the fission yeast *S. pombe* spore as a model system for studying the molecular mechanisms underlying the change in cytoplasmic fluidity during dormancy breaking. To evaluate the biophysical properties in the cytoplasm of the fission yeast spore, we first compared the motion of foreign tracer particles between vegetative cells and spores. Due to the rigid cell wall, it is technically challenging to inject tracer particles into fission yeast cells (31). To overcome this limitation, we used genetically encoded multimeric nanoparticles (GEMs), which self-assemble into a spherical particle with a diameter of 40 nm (hereafter referred to as 40nm-GEMs) (Fig. 1*A*) (12). The gene encoding 40nm-GEMs fused to a fluorescent protein, T-Sapphire, was introduced into the fission yeast, resulting in the formation of bright tracer particles in both vegetative cells and spores (Fig. 1*B* and Movie S1). The GEM particles were tracked to obtain trajectories and estimate the effective diffusion coefficient (D_{eff}) from the mean squared displacement (MSD) curves (*SI Appendix, SI Materials and Methods*). The median effective diffusion coefficient was 0.47 ± 0.10 $\mu m^2/s$ in vegetative cells (Fig. 1 *C* and *D*), which was comparable to the diffusion coefficient values in the previous studies using 40nm-GEMs in fission yeast vegetative cells (10, 32–34). As we expected, the median effective diffusion coefficient of 0.036 ± 0.0095 $\mu m^2/s$ in spores indicates that the 40nm-GEMs in spores were approximately 13 times less mobile compared with those in vegetative cells (Fig. 1 *C* and *D*). In addition, using the ensemble-averaged MSD curves of vegetative cells and spores (Fig. 1 *C*, *Inset*), we computed the anomalous exponent to be ~0.9 in vegetative cells and ~0.75 in spores. This means that the spore cytoplasm made the GEM motion strongly

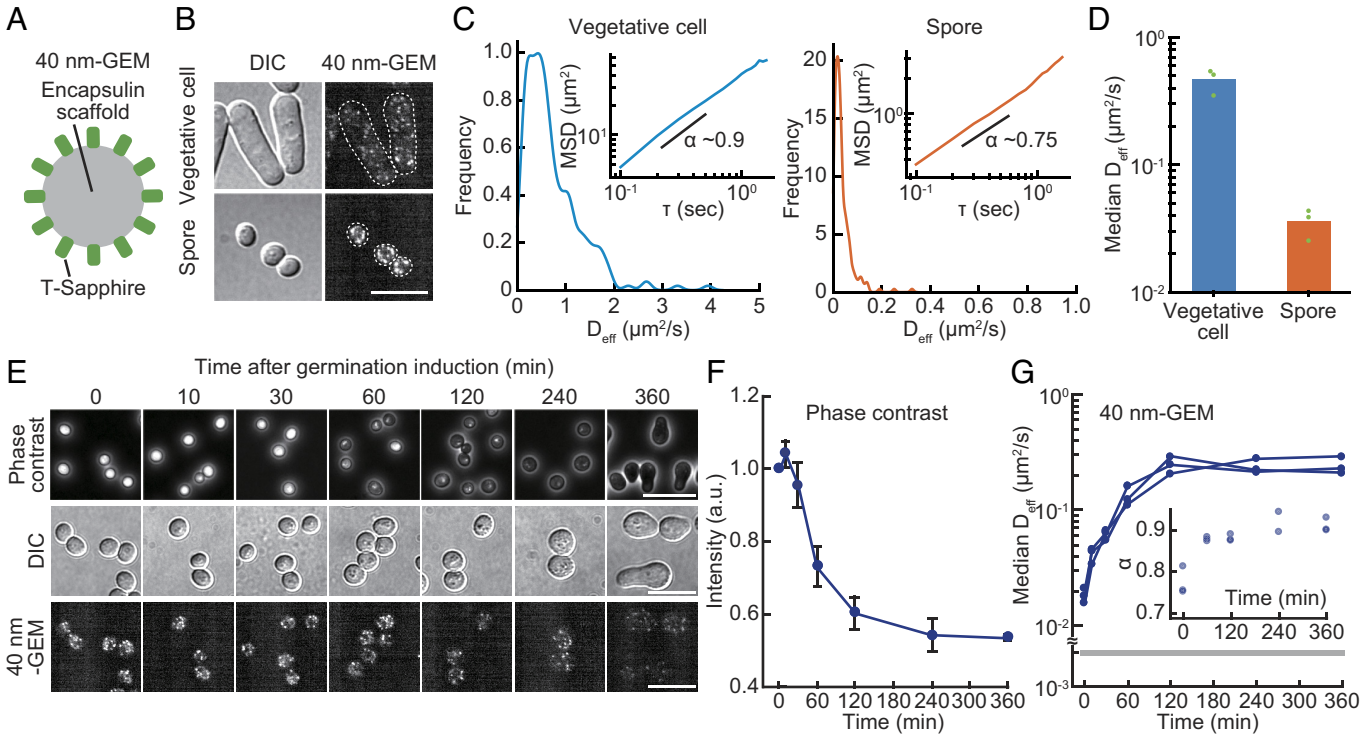

Fig. 1. The mobility of 40 nm particles is limited in fission yeast spores but increases rapidly during germination. (*A*) A schematic illustration of GEMs with a diameter of 40 nm (40nm-GEMs). (*B*) Representative differential interference contrast (DIC) (*Left*) and spinning disk confocal fluorescence images (*Right*) of vegetative cells (*Upper*) and spores (*Lower*) of fission yeast expressing 40nm-GEMs. (Scale bar, 10 μm.) (*C*) Distribution of effective diffusion coefficients (D_{eff}) for 40nm-GEMs in vegetative cells (*Left*) (n = 218) and spores (*Right*) (n = 221). The *Inset* indicates the ensemble-averaged MSD curves of 40nm-GEMs for vegetative cells (*Left*) and spores (*Right*). (*D*) Median D_{eff} of 40nm-GEMs in vegetative cells and spores. Each dot indicates the median D_{eff} from three independent experiments, and bars are their means. (*E*) Representative phase contrast images (*Upper*) of cells expressing 40nm-GEMs at the indicated time after germination initiation upon glucose refeeding. Also shown are DIC (*Middle*) and confocal fluorescence images (*Lower*) under the same condition. (Scale bar, 10 μm.) (*F*) Quantification of intensities of phase contrast images in spores during germination from three independent experiments. Each point represents the mean of the three independent experiments with SD. In each experiment, the mean intensities in spores from at least 125 cells were quantified. (*G*) Median D_{eff} of 40nm-GEMs during germination from three independent experiments (n > 300 trajectories for each experiment). The *Inset* indicates the anomalous exponent α during germination from three independent experiments. The gray line indicates the level of technical noise (~0.002 $\mu m^2/s$ both in vegetative cells and spores) as described in *SI Appendix*, Fig. S3.

subdiffusive; in other words, the GEM motion in spores was hindered by, for example, the enhanced macromolecular crowding and/or higher cytoplasmic viscoelasticity. After the spores were purified and stored at 4 °C, GEM mobility was measured over time. GEM mobility decreased slightly as the spores were stored at 4 °C (*SI Appendix*, Fig. S1 *A* and *B*), indicating that the GEM mobility does not substantially change during the storage of spores at 4 °C. These results show that the cytoplasmic fluidity in fission yeast spores is strongly restricted compared to that in vegetative cells.

The Mobility of 40 nm Particles Increases during the Initial Stage of Spore Germination. Next, we examined when the reduced GEM mobility in spores recovered during dormancy breaking. For induction of germination, spores were transferred to a glucose-rich medium. Consistent with previous reports (35–39), phase contrast microscopy indicated that the spore cytoplasm underwent a bright-to-dark transition approximately 1 h after induction, followed by spore swelling and germ tube elongation after 4 to 6 h (Fig. 1 *E* and *F*). We tracked the GEM particles and found that the effective diffusion coefficient rapidly increased by sevenfold within the first hour after induction and subsequently reached the same level as that in vegetative cells (Fig. 1*G*, *SI Appendix*, Fig. S2*A*, and Movie S2). We used ethanol-fixed cells/spores to confirm that the effective diffusion coefficient during germination (~0.01 to 0.1 $\mu m^2/s$) is above the technical noise level (~0.002 $\mu m^2/s$, gray line in Fig. 1*G* and *SI Appendix*, Fig. S3 *A–C*). The subdiffusive anomalous exponent also showed rapid recovery (Fig. 1 *G*, *Inset* and *SI Appendix*, Fig. S2*B*). The transition of phase-bright spores to phase-dark spores was observed in the phase contrast image 30 min after germination induction (Fig. 1*F*), whereas GEM mobility started to increase earlier than spore darkening (Fig. 1*G*). In other words, cytoplasmic fluidization precedes the bright-to-dark transition of spores under phase contrast microscopy, which has been traditionally the earliest hallmark of germination onset (35) and signaling dynamics (37, 40).

Glucose-Sensing via the cAMP-PKA Pathway is Essential for the Increase in the Mobility of 40 nm Particles during Germination. To investigate the molecular mechanism underlying the observed increase in GEM mobility in the early phase of germination (Fig. 1*G*), we first focused on glucose-sensing via the cAMP-PKA pathway (Fig. 2*A*) (41–43). Glucose is recognized by a G-protein coupled receptor, Git3, at the plasma membrane, thereby activating the adenylate cyclase, Cyr1 (Fig. 2*A*). The activated Cyr1 produces cAMP, which binds to the PKA regulatory subunit, Cgs1, and finally activates the PKA catalytic subunit, Pka1(Fig. 2*A*). This pathway is known to play a critical role in the initiation of germination in fission yeast spores (35). Indeed, in the strains *pka1*Δ and *cyr1*Δ, these spores did not exhibit any bright-to-dark transition (Fig. 2*B*) or germ tube elongation (Fig. 2*C*) even 15 h after the addition of glucose. We therefore examined whether the cAMP-PKA pathway is required for the increase in the GEM mobility, which precedes the canonical early events of germination such as bright-to-dark transition and germ tube elongation. We found that the GEM mobility remained unchanged in mutant strains lacking cAMP-PKA pathway components (*git3*, *cyr1*, or *pka1*) up to 6 h after germination induction (Fig. 2*D*). We also confirmed no significant differences in the median diffusion coefficient and anomalous exponent during vegetative growth among these mutant strains (*SI Appendix*, Fig. S4 *A–C*). These results indicate that the activation of the cAMP-PKA pathway in response to glucose is necessary for the increase in the GEM mobility during germination.

Germination-Induced Changes in Particle Assembly, Cellular Volume, Protein Synthesis, and Cytoskeletal Dynamics Have No Impact on the Increase in the Mobility of 40 nm Particles. In addition to the cAMP-PKA pathway, we explored other possible mechanisms affecting the mobility of 40nm-GEMs during germination. We first examined the change in particle assembly during the germination. The fluorescence intensity of each single particle appeared to decrease in spores as the

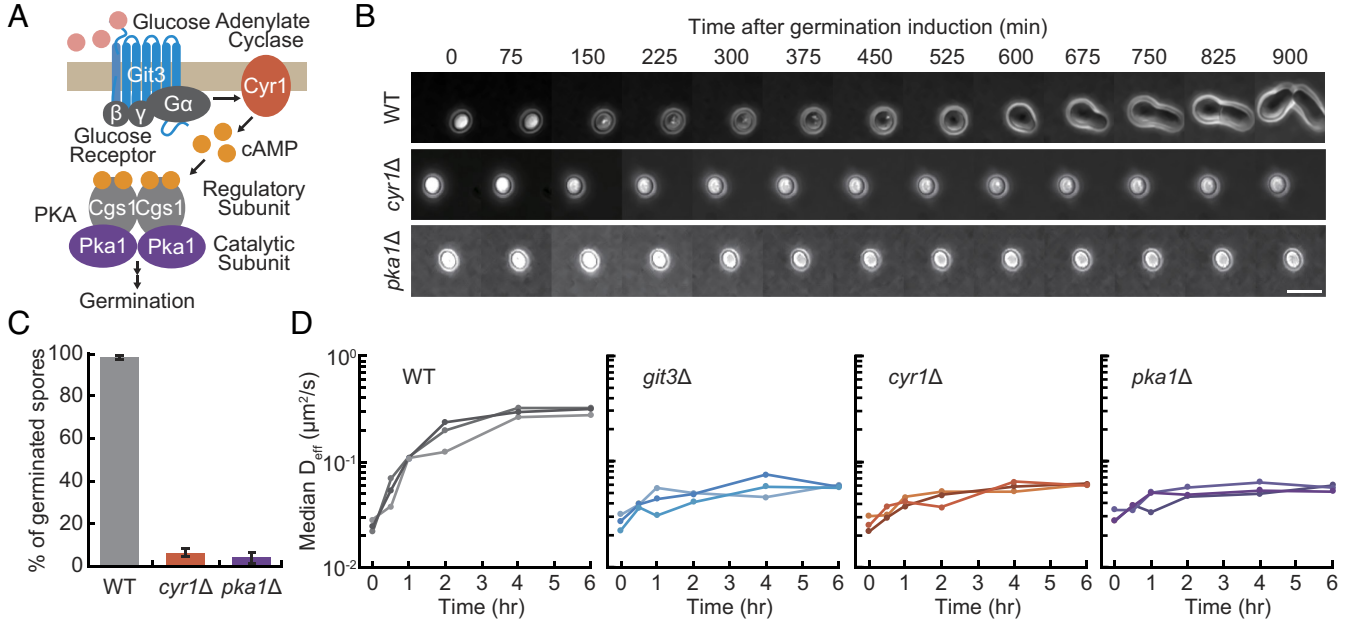

Fig. 2. The cAMP-PKA pathway is required for the increase in the mobility of 40 nm particles during spore germination. (*A*) A schematic illustration of the cAMP-PKA pathway upon glucose stimulation in fission yeast. (*B*) Representative phase contrast images of wild-type (WT, *Top*), *cyr1*Δ (*Middle*), and *pka1*Δ (*Bottom*) spores at the indicated time after germination induction. (Scale bar, 5 μm.) (*C*) Percentage of germinated spores showing an elongated germ tube at 15 h (900 min) after the glucose addition. The means and SDs were calculated from three independent experiments. In each experiment, at least 103 cells were used for quantification. (*D*) Median D_{eff} of 40nm-GEMs during germination in the wild-type (WT), *git3*Δ, *cyr1*Δ, and *pka1*Δ strains from three independent experiments (n > 340 trajectories for each experiment).

germination proceeded (Fig. 1*E*), which might reflect the change in multimerization and/or size of the GEM particles. To examine the effects on the increase in the GEM mobility, we quantified the fluorescence intensity of a single-GEM particle at different time points (0, 1, 2, 4, and 6 h) from germination in spores and in vegetative cells (*SI Appendix*, Fig. S5*A*). The distributions of fluorescence intensity of 40nm-GEMs in germinating spores and vegetative cells showed unimodal distribution, and their peaks shifted leftward as the germination proceeded (*SI Appendix*, Fig. S5*A*). Although 6 h after germination induction the average fluorescence intensity of particles was 1.5-fold less than before induction, the fluorescence intensity did not change within the first 2 h of germination induction (*SI Appendix*, Fig. S5 *A* and *B*). Importantly, the GEM mobility increased significantly within an hour of germination induction (Fig. 1*G*). From these results, we concluded that the rapid increase in the GEM mobility was not attributable to the change in particle assembly and/or size during germination.

Prior works have shown that a reduction in cellular volume decreases macromolecular mobility under hyperosmotic stress and nutrient starvation (10, 16, 18). Indeed, the cellular volume increases as the germination proceeds (Fig. 1*E*) (35, 37). We therefore asked whether the increase in cellular volume contributed to the increase in the GEM mobility after germination induction. For simplicity, we quantified cytoplasmic areas as a proxy for cellular volume using DIC (differential interference contrast) images of spores expressing 40nm-GEMs (Fig. 1*E*) and fluorescence images of spores expressing mNeonGreen (Fig. 3*A*). In both analyses of cell size, the cytoplasmic area of spores did not substantially change within 2 h after germination induction but increased thereafter (Fig. 3*B*). Given that the GEM mobility increased within 1 h from germination initiation (Fig. 1*G*), cytoplasmic fluidization precedes the spore swelling. Thus, these results strongly suggest that the increase in cytoplasmic volume during germination does not cause the increase in the GEM mobility in the early stage of germination.

Finally, we explored the effects of protein synthesis or cytoskeleton on the GEM mobility by using small chemical inhibitors. Treatment with a translation inhibitor, cycloheximide (CHX) (44), or a TOR inhibitor, Torin1 (45), did not change the effective diffusion coefficients of 40nm-GEMs during germination (Fig. 3 *C* and *D*). Meanwhile, both CHX and Torin1 blocked the swelling and germ tube formation caused by germination induction (Fig. 3*C*), indicating that protein synthesis is necessary for the processes of swelling and germ tube formation, but not for the increase in the GEM mobility in the earlier stage of germination. We next asked whether the cytoskeletal structure and/or dynamics influence the GEM mobility. Intracellular particle diffusion is known to be affected by cytoskeletons and molecular motors (12, 46). To examine these effects, we treated cells with an actin depolymerizer, latrunculin A (47), and/or microtubule-destabilizing agents, thiabendazole and carbendazim (48), but none of these compounds had any impact on the GEM mobility (Fig. 3*E*). The germ tube formation was inhibited by treatment with these drugs (Fig. 3*C*). These results demonstrate that the cytoskeletal changes make a negligible contribution to the increase in the GEM mobility during germination.

ATP Production via Glycolysis Contributes to an Increase in 40 nm Particle Mobility after 1 h of Germination. Previous studies have shown that adenosine triphosphate (ATP) depletion drastically reduces tracer particle diffusion in bacterial cells (7, 19, 46), yeast cells (7, 49), and mammalian cells (46). We therefore investigated whether de novo ATP synthesis affords the GEM mobility in the germination process. Previous studies reported that a glycolysis inhibitor decreased the ATP level in vegetative cells of *S. pombe* (50, 51). In light of these reports, we treated spores with an inhibitor of glycolysis, 2-deoxyglucose (2-DG) (51), which resulted in the inhibition of swelling and germ tube formation at 6 h after germination induction (Fig. 3*C*). This result indicates that ATP synthesis via glycolysis is required for the germination progression. Interestingly, the GEM mobility increased within an hour after germination induction even in the presence of 2-DG, but reached a plateau at a low level (Fig. 3*D*). These results indicate that the ATP synthesis via the glycolysis was not necessary for the GEM mobility immediately after germination initiation but was required from 1 h after germination initiation.

Trehalose Degradation Downstream of the cAMP-PKA Pathway Increases 40 nm Particle Mobility during Germination. Among the possible mechanisms for increased GEM mobility during germination, we focused on intracellular trehalose and glycogen amount. Trehalose is a disaccharide formed by a 1,1-glycosidic bond between two glucose molecules, while glycogen is a branched polysaccharide composed of thousands of glucose molecules. Trehalose and glycogen in spores accumulated nearly 1,000-fold and 40-fold compared to the level in vegetative cells, respectively (Fig. 4*A* and *SI Appendix*, Fig. S6*A*), which is consistent with previous reports (52, 53). We roughly estimated that the trehalose and glycogen concentrations in a fission yeast spore were approximately 5% and 4% w/v, respectively (*SI Appendix, SI Materials and Methods*). Recent studies have shown that vegetative cells of budding yeast respond to heat shock by accumulating trehalose and glycogen, which increase cytoplasmic viscosity and thus maintain a constant protein diffusion rate (23). Therefore, we hypothesized that the accumulation of trehalose and glycogen causes a decrease in cytoplasmic viscosity in spores and that their degradation triggers the cytoplasmic fluidization upon germination.

To investigate this hypothesis, we first quantified the amount of trehalose and glycogen in fission yeast spores during germination. We found that trehalose was rapidly degraded at the same time as the increase in the GEM mobility (Fig. 4*B*). On the other hand, glycogen began to decrease 2 h after germination induction (*SI Appendix*, Fig. S6*B*). These results suggest that the degradation of trehalose, but not glycogen, could contribute to an increase in GEM mobility during early spore germination. Therefore, we focused on the relationship between trehalose degradation and GEM mobility hereafter. We measured the trehalose amount and the GEM mobility in a mutant strain lacking *ntp1*, a trehalase gene (54). We found that *ntp1*-deleted cells (*ntp1*Δ) did not show the rapid decrease in trehalose amount within 1 h of germination induction observed in WT cells, and their trehalose amount remained constant up to 8 h after germination induction (Fig. 4*C*). Additionally, in spores lacking *pka1*, trehalose degradation was suppressed after germination induction (Fig. 4*C*), implying that the cAMP-PKA pathway controls the trehalose degradation pathway. We also found that the germination process was severely delayed in the *ntp1*Δ strain, which is incapable of forming a germ tube 8 h after germination (Fig. 4*D*), consistent with a previous report (53). Importantly, the increase in GEM mobility was substantially suppressed in the *ntp1*Δ strain compared to the WT after germination induction (Fig. 4*E*). We confirmed that there were no significant differences in GEM mobility during vegetative growth between WT and *ntp1*Δ strains (*SI Appendix*, Fig. S4 *A–C*). These results suggest that Ntp1-mediated trehalose degradation is required for cytoplasmic fluidization and rapid germination through the cAMP-PKA pathway.

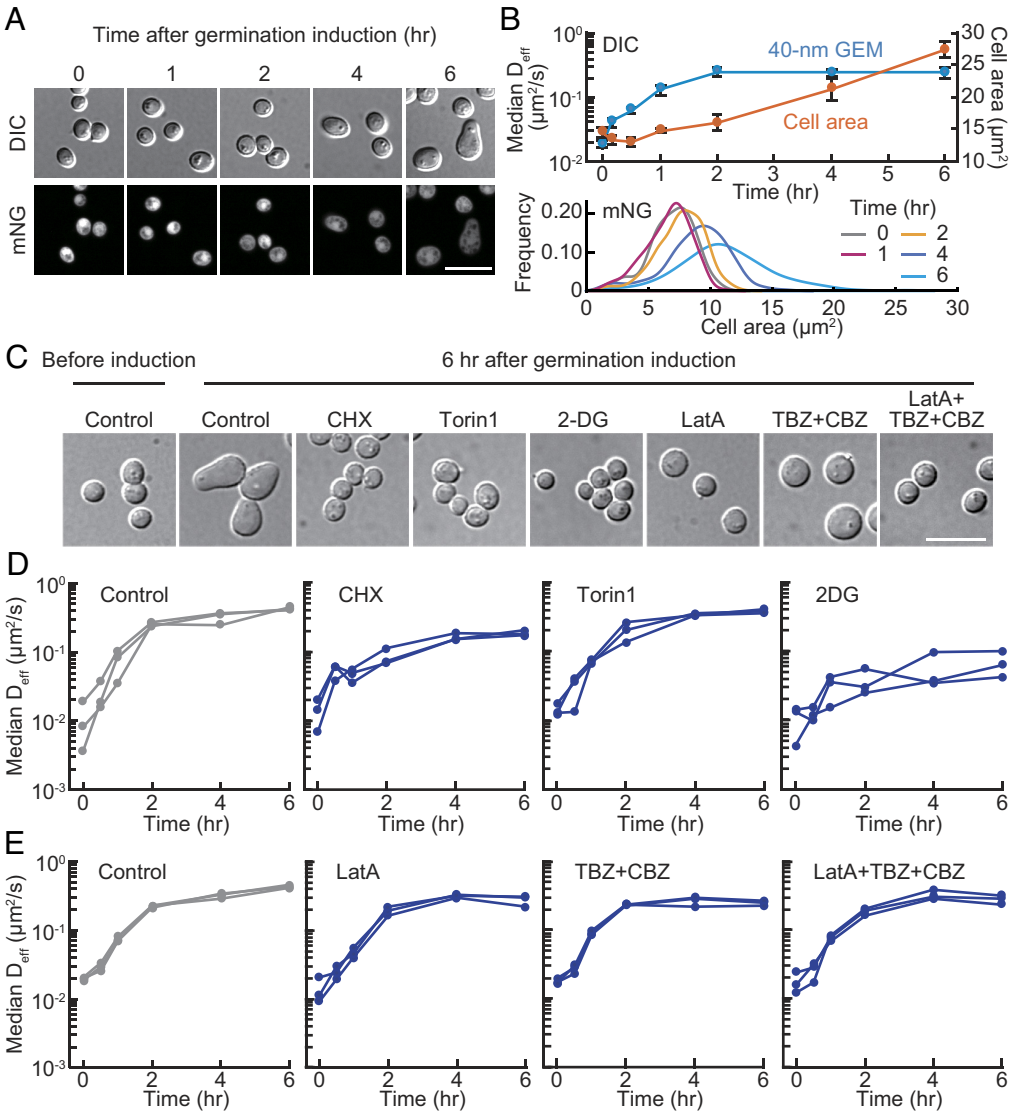

Fig. 3. Effect of changes in cellular volume, protein synthesis, cytoskeletal dynamics, and glycolysis on 40 nm particle mobility during germination. (*A*) Representative DIC (*Upper*) and confocal fluorescence images (*Lower*) of cells expressing mNeonGreen (mNG) under the constitutive promoter *Padh1* during germination. (Scale bar, 10 μm.) (*B*) Cell areas measured using DIC or mNG images during germination. (*Upper*) The blue and orange lines indicate the GEM mobility calculated as the mean of the three median D_{eff} values as shown in Fig. 1*G* and the mean cell area from three independent experiments, respectively. For the quantification of cell area, mean values are used to summarize each experiment from three replicates. Error bars represent SD. (*Lower*) The distribution of cell areas at the indicated time point after germination induction was shown (n > 500 cells at each time point). Note that there is a difference in cell area values between DIC- and mNG-based measurements because the cell contours were quantified in addition to the cytoplasm in the DIC images. (*C*–*E*) Effect of various types of inhibitors on germination progression and GEM mobility. (*C*) Representative DIC images of germinating spores at 0 h and 6 h after glucose addition in the absence or presence of cycloheximide (CHX), Torin1, 2-deoxyglucose (2-DG), latrunculin A (LatA), thiabendazole (TBZ), and carbendazim (CBZ). (Scale bar, 10 μm.) (*D*) Median D_{eff} of 40nm-GEMs during germination in the presence of CHX, Torin1, 2-DG (n > 180 trajectories for each experiment). (*E*) Median D_{eff} of 40nm-GEMs during germination in the presence of LatA, TBZ and/or CBZ (n > 180 trajectories for each experiment).

We recognized that a small fraction of spores in the *ntp1*Δ strain displayed swelling, an initial feature of germination, 8 h after germination induction (Fig. 4*D*, yellow arrow). This result could be due to the Ntp1-independent trehalose degradation in this small population of spores, resulting in the progression of germination. Indeed, the quantification of the effective diffusion coefficients of 40nm-GEMs at the single-spore level revealed that approximately one-fifth of *ntp1*Δ spores showed an increase in the GEM mobility comparable to wild-type (WT) spores 6 h after germination induction (Fig. 4*F*). These *ntp1*Δ spores with increased GEM mobility were larger in cell size than the spores with low GEM mobility (Fig. 4*F*). Consistent with these results, the trehalose amount decreased even in *ntp1*Δ spores 24 h after the germination induction, while it remained unchanged in *pka1*Δ spores (Fig. 4*G*). Taken together, these results lead us to propose the existence of at least two trehalose degradation pathways during the spore germination of fission yeast; one is Ntp1-dependent fast trehalose degradation, whereas the other is Ntp1-independent slow trehalose degradation (Fig. 4*H*). Both trehalose degradation pathways are controlled by the cAMP-PKA pathway (Fig. 4*H*). We note that the former pathway, Ntp1-dependent fast trehalose degradation, is necessary for rapid germination in response to glucose stimulation.

Overexpression of Trehalase in Spores Deficient in the cAMP-PKA Pathway Partially Increases the Mobility of 40 nm Particles during Germination. We next examined whether Ntp1 overexpression is sufficient to increase the GEM mobility and induce germination. First, we developed a spore-specific gene expression system in fission yeast cells by using promoters whose expression was specifically induced after the completion of the sporulation process. By reanalyzing previously reported microarray data during sporulation in fission yeast cells (55), we identified

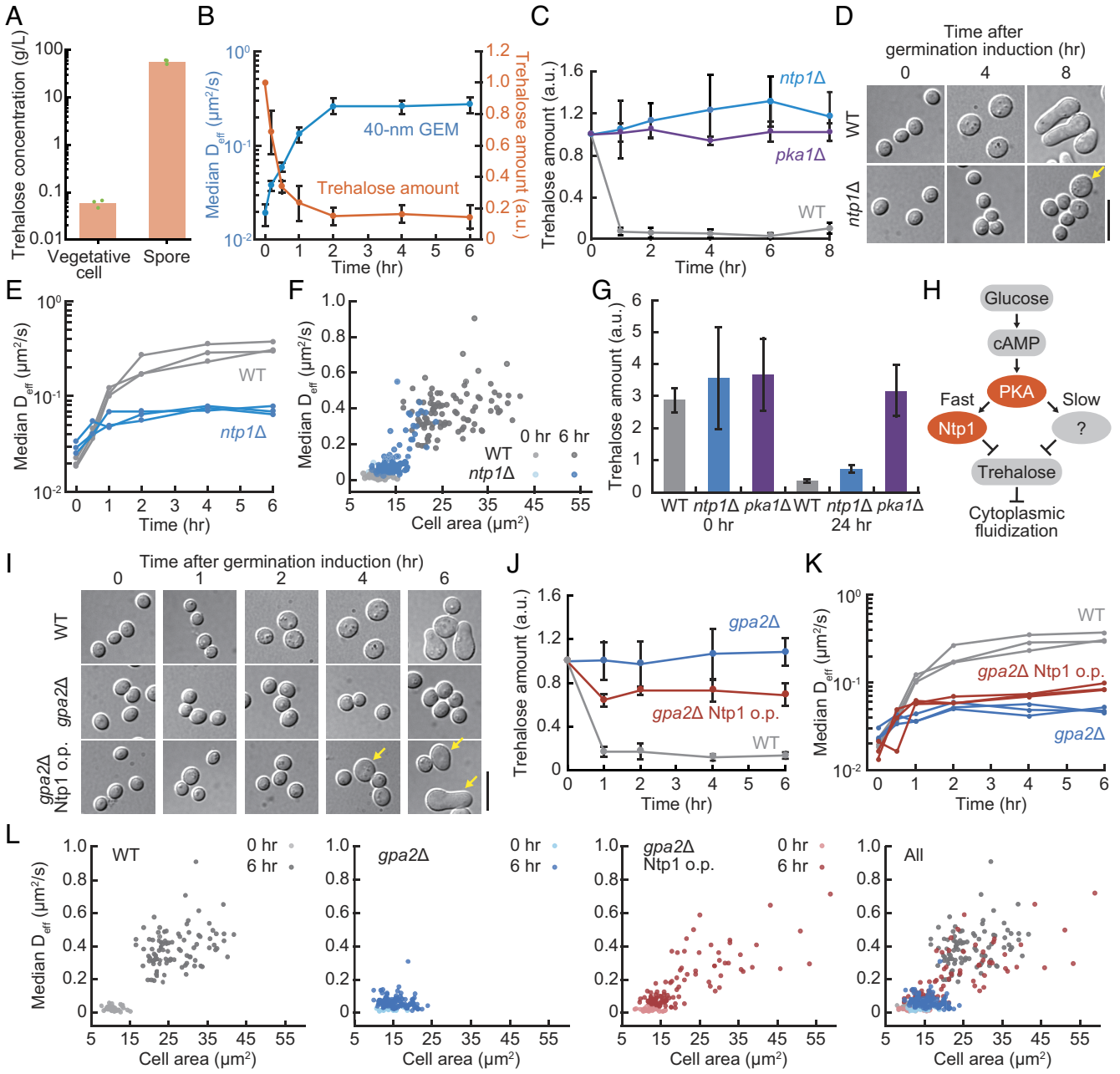

Fig. 4. Trehalose degradation through the cAMP-PKA pathway is required for the increase in the mobility of 40 nm particles. (*A*) Quantification of the trehalose concentration in vegetative cells and spores. Mean values were calculated from three independent experiments, each indicated by a green dot. (*B*) Time courses of GEM mobility and trehalose amount at the indicated time after germination induction. A blue line indicates the GEM mobility calculated as the mean of the three median D_{eff} values in Fig. 1*G*. An orange line indicates the trehalose amount, which was the mean from three independent experiments. Error bars represent SD. (*C*) Trehalose amount in wild-type (WT), *ntp1*Δ, and *pka1*Δ spores at the indicated time after germination induction. Each line indicates the mean value from three independent experiments. Error bars represent SD. (*D*) Representative DIC images of WT (*Upper*) and *ntp1*Δ (*Lower*) at the indicated time after germination induction. The yellow arrow indicates swollen spores of the *ntp1*Δ strain. (Scale bar, 10 μm.) (*E*) Median D_{eff} of 40nm-GEMs during germination in WT and *ntp1*Δ spores from three independent experiments (n > 460 trajectories for each experiment). (*F*) Median D_{eff} of 40nm-GEMs and cell areas at the single-spore level for WT and *ntp1*Δ strains. Each dot represents the median D_{eff} of 40nm-GEMs and cell area in the same cell (n = 30 cells at 0 h and n = 90 cells at 6 h from three independent experiments). Cell areas were quantified by using DIC images. (*G*) Trehalose amounts in the WT, *ntp1*Δ, and *pka1*Δ strains at 0 h and 24 h after germination induction. Mean values from three independent experiments are shown with error bars (SD). (*H*) A schematic model of the glucose-sensing and trehalose degradation pathways after germination initiation upon glucose refeeding. PKA activation leads to trehalose degradation via Ntp1-dependent and -independent pathways, resulting in cytoplasmic fluidization and germination. (*I*) Representative DIC images of spores of WT (*Upper*), *gpa2*-deficient mutant (*gpa2*Δ; *Middle*), and *gpa2*-deficient mutant expressing Ntp1 under the spore-inducible promoter *Posi2* (*gpa2*Δ Ntp1 o.p.; *Lower*) upon germination induction. Yellow arrows indicate swollen spores starting to germinate. (Scale bar, 10 μm.) (*J*) Trehalose amount in WT, *gpa2*Δ, and *gpa2*Δ Ntp1 o.p. spores at the indicated time after germination induction. Each line indicates the mean value from three independent experiments. Error bars represent SD. (*K*) Median D_{eff} of 40nm-GEMs during germination in WT, *gpa2*Δ, and *gpa2*Δ Ntp1 o.p. spores from three independent experiments (n > 460 trajectories for each experiment). (*L*) Median D_{eff} of 40nm-GEMs and cell areas at the single-spore level for WT, *gpa2*Δ, and *gpa2*Δ Ntp1 o.p. strains. Each dot represents the median D_{eff} of 40nm-GEMs and cell area in the same cell (n = 30 cells at 0 h and n = 90 cells at 6 h from three independent experiments). Cell areas were quantified by using DIC images. Of note, the WT data are the same as those of panel *F*.

the top four genes (*SPAC869.09*, *hry1*, *isp3*, and *pdc202*) whose expression was strongly induced in spores compared to vegetative cells. The region approximately 1,000 bp upstream of those genes was used as the promoter region to express a certain gene in spores. We named these promoters *Posi1–4* (Promoters for only spore induction), respectively. We quantified the expression levels of

mNeonGreen under *Posi1–4* (*SI Appendix*, Fig. S7 *A–D*), and found that *Posi2* showed the highest ratio of the expression of mNeonGreen in spores to that in vegetative cells (*SI Appendix*, Fig. S7*E*). Therefore, we used *Posi2* for the following experiment.

To investigate whether Ntp1 overexpression suffices to induce germination, we established and analyzed spores overexpressing Ntp1 under *Posi2*. However, the spores overexpressing Ntp1 did not show any morphological change in the absence of glucose and exhibited an accelerated increase in the GEM mobility upon glucose stimulation. Therefore, we next overexpressed Ntp1 in spores deficient in the cAMP-PKA pathway and treated the spores with glucose in order to examine the effects of Ntp1 overexpression on glucose-induced morphological change and GEM mobility. Spores lacking *gpa2*, the gene encoding heterotrimeric G-protein alpha subunit (Fig. 2*A*), which mediates the glucose receptor and the cAMP-PKA pathway, demonstrated a significant delay in swelling upon glucose stimulation (Fig. 4*I*), as seen in *pka1*- or *cyr1*-deleted spores (Fig. 2 *B* and *C*). Meanwhile, the overexpression of Ntp1 in spores lacking *gpa2* partially rescued the glucose-induced germination, namely swelling (Fig. 4*I*, yellow arrows). In addition, by overexpressing Ntp1, intracellular trehalose was partially degraded during germination (Fig. 4*J*), and the GEM mobility was also partially increased at the population level (Fig. 4*K*). The cell-to-cell heterogeneity of germination in *ntp1Δ* spores (Fig. 4 *D* and *F*) prompted us to investigate the correlation between GEM mobility and cell size at the single-cell level (Fig. 4*L*). In WT strain, all spores showed increased GEM mobility and swelling at 6 h after germination induction (Fig. 4*L*, WT), while in *gpa2*-deficient strain most spores indicated neither the increase in GEM mobility nor the increase in cell area after the germination induction (Fig. 4*L*, *gpa2*Δ). The Ntp1-overexpressing strain exhibited considerable cell-to-cell heterogeneity; approximately one-third of spores exhibited both increased GEM mobility and swelling at 6 h after the induction, comparable to the WT strain (Fig. 4*L*, *gpa2*Δ Ntp1 o.p. and All). We further confirmed that some of Ntp1-overexpressing spores showed normal cell division and mitosis after germination induction, similar to the WT strain (*SI Appendix*, Fig. S8 *A* and *B*). These results suggest that Ntp1 activity alone can induce cytoplasmic fluidization and subsequent germination events even without the glucose-sensing pathway.

The Mobility of 50 to 150 nm Particles Also Decreases in Spores and Increases at the Onset of Germination. To gain further insight into the spore cytoplasm, we examined the size dependency of particle diffusion, which reflects the spatial scales of cytoplasmic structures (12, 56, 57). We first observed the mobility of particles with size larger than 40nm-GEMs by using μNS, which self-assembles into particles of different sizes (50 to 150 nm) (19, 58). In both vegetative cells and spores, μNS were observed as particles of varying size and brightness (Fig. 5*A*). We then analyzed the μNS particles with fluorescence intensities lower than a certain threshold to mitigate the effects of size variability (*SI Appendix*, Fig. S9*A*). The effective diffusion coefficients were 0.012 ± 0.0025 $\mu m^2/s$ and 0.00088 ± 0.00011 $\mu m^2/s$ in vegetative cells and spores, respectively, indicating that the mobility of μNS, similarly to that of 40nm-GEMs, was strongly restricted in spores (Fig. 5*B*). During the germination process, the μNS mobility was gradually increased (Fig. 5*C*), which is consistent with a previous report on budding yeast spores (24). Within the first 2 h of germination, μNS mobility increased about twofold, followed by a gradual increase in μNS mobility. We also quantified the anomalous exponent during germination from the ensemble-averaged MSD curves (Fig. 5 *C*, *Inset* and *SI Appendix*, Fig. S9*B*). Compared with the 40nm-GEMs, the μNS in spores exhibited a much smaller anomalous exponent value, α ~0.3 to 0.5.

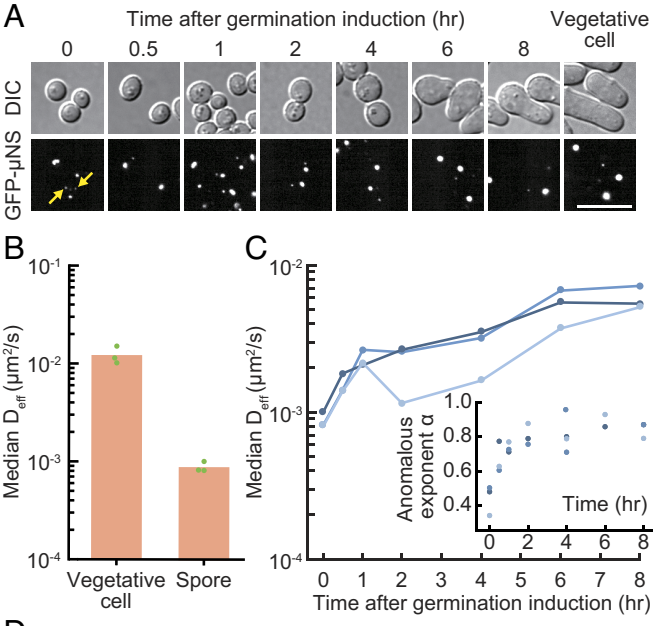

D

	Vegetative cell	Spore	Ratio
FCS (mNG, 5 nm)	39.3 ± 10.2 μm²/s	10.2 ± 2.3 μm²/s	3.8
FRAP (mNG, 5 nm)	15.2 ± 4.6 μm²/s	0.61 ± 0.21 μm²/s	25.0
Particle tracking (GEM, 40 nm)	0.47 ± 0.10 μm²/s	0.036 ± 0.0095 μm²/s	13.0
Particle tracking (μNS, 50-150 nm)	0.012 ± 0.0025 μm²/s	0.00088 ± 0.00011 μm²/s	13.9

Fig. 5. The mobility of particles of different sizes in spores and vegetative cells. (*A*) Representative DIC (*Upper*) and confocal fluorescence images (*Lower*) of fission yeast cells expressing μNS at the indicated time after germination induction. Yellow arrows indicate the small size particles (*SI Appendix*, Fig. S9*A*), which are used for the estimation of the effective diffusion coefficient of μNS. (Scale bar, 10 μm.) (*B*) Median D_{eff} of μNS in vegetative cells and spores. Each dot indicates the median D_{eff} from three independent experiments, and bars are their means. (*C*) Median D_{eff} of μNS during germination from three independent experiments (n > 30 trajectories for each experiment). The *Inset* indicates anomalous exponent α during germination. (*D*) Summary of effective diffusion coefficients for particles of various sizes in vegetative cells and spores. "Ratio" indicates the ratio of the effective diffusion coefficients of vegetative cells to those of spores.

This result indicates that, in spores, the μNS particles were severely restricted in the time scale of observation. To provide further support for this idea, we computed velocity autocorrelation functions (VAFs) (*SI Appendix*, Fig. S9 *C–H*), which were used as a diagnostic tool to explore the underlying mechanism of intracellular subdiffusion (7, 59). The VAFs of the spore cytoplasm showed sharper negative peaks compared to those of cells 1 h after germination induction or vegetative cells (*SI Appendix*, Fig. S9, and H). These results suggest that the μNS particles are locally confined and their motion is caused by their bouncing off elastic structures as they collide with them.

Fluorescent Protein–Sized Particles Diffuse throughout the Spore Cytoplasm within a Time Frame on the Order of Seconds. Although the diffusion of 40nm-GEMs and μNS was drastically restricted in the spore cytoplasm (Figs. 1*D* and 5*B*), it remains unclear whether smaller proteins are also affected by the change in the biophysical properties of spores. To investigate this, we quantified the effective diffusion coefficients of the

green fluorescent protein mNeonGreen (mNG, around 3 nm in size), which is smaller than 40nm-GEMs. We first observed the movement of mNG by using fluorescence correlation spectroscopy (FCS). FCS is a technique used to estimate the effective diffusion coefficient in a confocal volume (~1 fL) by observing the fluctuation of fluorescent molecules (60–62). In the FCS analysis, we measured the time series of mNG intensity in vegetative cells and spores of fission yeast and obtained autocorrelation functions (*SI Appendix*, Fig. S10 *A* and *B*). The effective diffusion coefficient of mNG in spores was about fourfold reduced compared to that in vegetative cells (Fig. 5*D* and *SI Appendix*, Fig. S10*C*). For further examination, we used fluorescence recovery after photobleaching (FRAP) to estimate the effective diffusion coefficient of mNG. In vegetative cells, the estimated effective diffusion coefficients of mNG-based on FCS and FRAP were close to each other (Fig. 5*D* and *SI Appendix*, Fig. S10*E*). In spores, we found that the mNG diffusivity obtained from FRAP was much lower than that from FCS (Fig. 5*D* and *SI Appendix*, Fig. S10*E*). Potential mechanisms underlying the discrepancy between FCS and FRAP include inhomogeneous diffusivity and/or binding to immobile intracellular structures (63, 64), although determining the precise mechanism for the spore cytoplasm requires further investigation. Note that, even in the FRAP analysis, mNG diffused throughout the spore cytoplasm within the order of seconds (*SI Appendix*, Fig. S10*D*). Based on these results, it is proposed that small signaling proteins, such as the cAMP-PKA pathway and Ntp1, are relatively free to diffuse in the spore cytoplasm and have the ability to transmit dormancy-breaking signals after the glucose addition, while the motion of large protein complexes is restricted.

Discussion

Growing evidence indicates that a liquid-like cytoplasmic property turns into a solid- or glass-like state under stress conditions, and these cytoplasmic changes have been proposed to be responsible for stress resistance and dormancy breaking (7, 24). However, the molecular basis underlying such changes in the cytoplasmic properties in response to environmental stimuli is not yet fully understood. In this study, we focused on the germination of fission yeast spores as a model system of dormancy breaking. By using genetically encoded tracer particles, we found that the spore cytoplasm markedly hinders intracellular diffusion, and rapidly fluidizes upon germination induction. The cytoplasmic fluidization during germination is mediated by the degradation of intracellular trehalose. Furthermore, we revealed the signaling pathway responsible for the trehalose degradation—namely, glucose is recognized by Git3, resulting in activation of the cAMP-PKA pathway and Ntp1. These events in germination have been summarized in the model (Fig. 6*A*).

We examined the mobility of three types of particles of different sizes in the spore cytoplasm as summarized in Fig. 6*B*. First, although the diffusivity of mNG in spores was reduced, mNG can still diffuse throughout the spore cytoplasm within a time frame on the scale of seconds (*SI Appendix*, Fig. S10*D*). This result indicates that signaling molecules such as PKA and Ntp1 diffuse relatively freely even in the spore cytoplasm and can respond rapidly to external signals for dormancy breaking. The large discrepancy between the FRAP- and FCS-based estimates of mNG diffusivity in spores (Fig. 5*D*) might reflect a spore-specific cytoplasmic state because the cytoplasm of vegetative cells did not produce such a discrepancy. An interesting possibility is the presence of immobile binding traps, which have been theoretically investigated to reconcile disparate estimates of the diffusion coefficient of Bicoid morphogen in *Drosophila* embryos (63, 65). Second, we found a marked reduction in the effective diffusion coefficients of 40nm-GEMs and strong subdiffusion of those

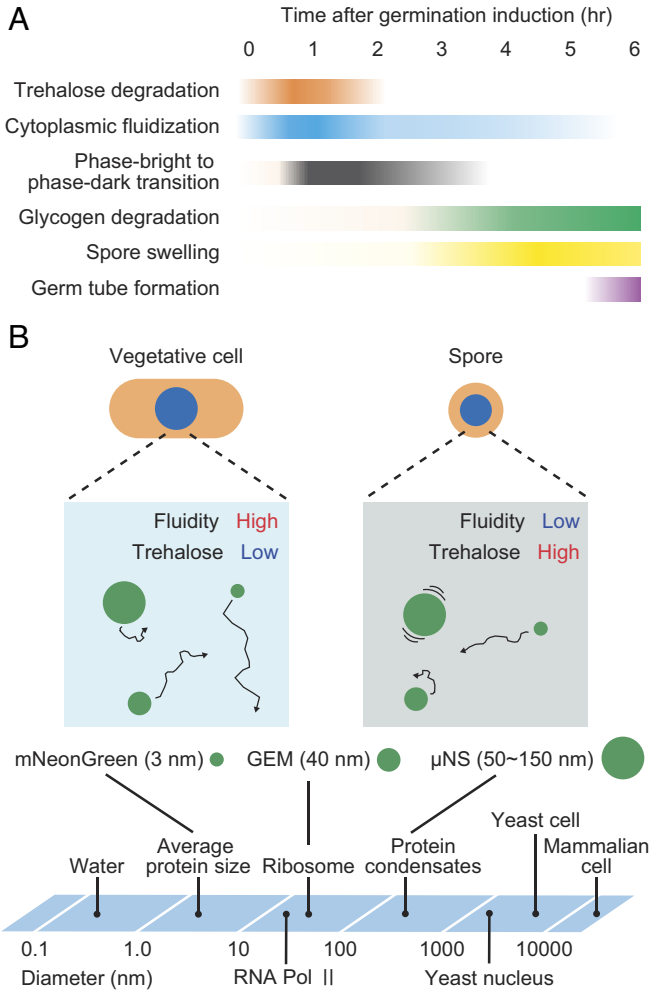

Fig. 6. Cytoplasmic fluidization is the initial event of the spore germination. (*A*) The schematic illustration of the timing of the events in early spore germination (0 to 6 h after glucose addition). Each timing of the event is based on the results of Fig. 4*B* (trehalose degradation), Fig. 1*G* (cytoplasmic fluidization, 40nm-GEMs) and Fig. 5*C* (cytoplasmic fluidization, μNS), Fig. 1*F* (phase-bright to phase-dark transition), *SI Appendix*, Fig. S6*B* (glycogen degradation), Fig. 3*B* (spore swelling), and Fig. 1*E* (germ tube formation). (*B*) A model of cytoplasmic properties in vegetative cells and spores of fission yeast. The amount of trehalose plays a key role in regulation of the cytoplasmic properties in fission yeast cells. Vegetative cells contain only a small amount of cytoplasmic trehalose, and mNG (~3 nm), 40nm-GEMs (~40 nm), and μNS (~50 to 150 nm) are free to diffuse in the cytoplasm. On the other hand, in spores, trehalose is highly accumulated, resulting in a decrease in the mobility of these particles. The mobility of 40nm-GEMs and μNS is strongly limited in the spore cytoplasm, while mNG are allowed to diffuse relatively freely throughout the cytoplasm.

particles in spores (Fig. 1 *D* and *G*). These results mean that the mobility of large complexes such as the ribosome (~30 nm) is severely limited in spores. Recently, in vitro experiments using *E. coli* and *Xenopus* cytoplasms demonstrated that an overcrowded cytoplasm can suppress ribosome mobility and thereby translational activity (66, 67). It is likely that the cytoplasmic biophysics of spores also suppresses the translational activity. The decrease in protein synthesis may allow spores to avoid wasting energy sources (e.g., ATP) and substrates (e.g., amino acids, nucleic acids), thus enabling their prolonged survival without nutrients. Third, the μNS particles in spores exhibited a drastic reduction in an anomalous exponent (Fig. 5*C*). This is consistent with previous studies showing that large structures such as protein condensates (~200 to 1,000 nm) and organelles (~100 to 1,000 nm) are immobilized in energy-depleted and nutrient-starved yeast cells (7, 18–20). Of note, the anomalous exponent of μNS (50~150 nm) in spores (α ~0.3 to 0.5) is even smaller than that in

energy-depleted yeast cells (α ~0.6) (7). This indicates that the spore cytoplasm is an extreme environment, and probing its material properties such as viscoelasticity could pave the way for a deeper understanding of the stress resistance achieved by the spores.

Trehalose has been well characterized as a protein protectant and a viscosity agent in vitro (68). Several pioneering works have suggested the involvement of trehalose in the regulation of cytoplasmic biophysics in vivo (23, 69, 70). Our study shows that trehalose accumulates in spores at a concentration of 5% w/v (Fig. 4*A*), and trehalose is rapidly degraded by germination induction (Fig. 4*B*), resulting in a 20-fold increase in GEM mobility. Furthermore, depletion of an enzyme that degrades trehalose, Ntp1, was shown to inhibit the increase in the GEM mobility upon germination induction (Fig. 4*E*). These results imply a direct link between trehalose and cytoplasmic fluidity. However, even in a 45% trehalose solution, the diffusion rate of purified GFP was reported to be only about twofold lower than that in a water solution (23). Therefore, trehalose as a simple viscogen cannot explain the decrease in the GEM mobility in fission yeast spores. We propose a model in which the trehalose forms spore-specific intracellular structures by interacting with other intracellular components. For example, it has been reported that a mixture of proteins in addition to trehalose can cooperatively increase the viscosity of a solution (71). Future studies should explore the physical chemistry of complex solutions of trehalose with proteins, lipids, and nucleic acids.

We found that glucose-triggered cAMP-PKA-Ntp1 signaling is required for cytoplasmic fluidization during germination. How is Ntp1 regulated downstream of PKA signaling in spores? There was no apparent effect of translation inhibition (CHX treatment) on the GEM mobility during germination (Fig. 3*D*), suggesting that PKA and Ntp1 are already expressed in spores and their activities are regulated posttranslationally during germination. These speculations can account for the fact that spore cytoplasm could not be fully fluidized merely by overexpressing Ntp1 in the cAMP-PKA pathway-deficient spores (Fig. 4 *K* and *L*). Consistent with these ideas, it has been reported that PKA-dependent phosphorylation activates trehalase Ntp1 in fission yeast and its budding yeast ortholog Nth1 (72, 73). Additionally, Ntp1 has a consensus site (S71) for PKA-dependent phosphorylation, and replacing S71 with an alanine residue results in loss of trehalase activity (74). However, it remains controversial whether PKA directly activates Ntp1 via phosphorylation (73–75). Future research should investigate the relation between PKA phosphorylation and Ntp1 trehalase activity in in vitro experiments.

By using foreign tracer particles, our study revealed that the biophysical properties of spores are quite different from those of vegetative cells. In addition to these exogenous particles, it would be interesting to investigate the mobility of endogenous proteins of different sizes in spores, as was recently done in a study on bacterial cells (76), because various features of proteins, such as charge and hydrophobicity, influence their mobility. In addition, the motions of intracellular particles are affected by both cytoplasmic viscoelasticity and active forces generated from molecular motors and metabolic reactions. However, in this study we relied on passive observations of the motion of probe particles, and thus we were not able to distinguish between the relative contributions of the passive and active mechanisms. A solution to this limitation would be to compare passive measurements with active microrheological measurements, in which the probe particles are controlled exogenously by optical tweezers or other means (46, 77). The prospect of applying such an approach to the spore cytoplasm is intriguing, although active microrheology experiments for yeast cells are still challenging at this time because the cell wall hinders the injection of specialized particles. Future studies will need to examine the cytoplasmic biophysics of dormant cells and how it regulates intracellular processes and functions.

Materials and Methods

Plasmids and Fission Yeast Strains. All plasmids and fission yeast strains used in this study are summarized in *SI Appendix*, Tables S1 and S2, respectively. The details are described in *SI Appendix, SI Materials and Methods*.

Live-Cell Fluorescence Imaging of Fission Yeast Cells. Fission yeast cells were imaged with an IX83 inverted microscope (Olympus) equipped with an sCMOS camera (ORCA-Fusion BT; Hamamatsu Photonics) and a spinning disk confocal unit (CSU-W1; Yokogawa Electric Corporation). Cells expressing 40nm-GEMs and μNS were excited with a 488 nm laser and recorded every 100 ms for 10 s and 500 ms for 2 min, respectively. The details are described in *SI Appendix, SI Materials and Methods*.

Quantification of Trehalose Amount. The amount of trehalose was measured using a Trehalose Assay kit (K-TREH; Megazyme) with reference to the previously reported method (23). The details are described in *SI Appendix, SI Materials and Methods*.

FCS and FRAP Measurement in Fission Yeast Cells. In FCS, mNG-expressing cells were imaged with a Leica SP8 Falcon confocal microscope equipped with an objective lens, HC PL APO 63×/1.20 W motCORR CS2. In FRAP, mNG-expressing cells were imaged with an FV3000 laser-scanning confocal microscope (Olympus) equipped with a UPLXAPO 60× objective lens, (NA = 1.42, WD = 0.15 mm; Olympus). Cells were excited with a 488 nm laser. The details are described in *SI Appendix, SI Materials and Methods*.

Data, Materials, and Software Availability. Imaging data have been deposited in SSBD (78).

ACKNOWLEDGMENTS. We thank all members of the Aoki Laboratory for their helpful discussions and assistance. We also thank members of the Tokai Tor Conference for the general discussion. Some fission yeast strains were provided by the National Bio-Resource Project, Japan, and others were a kind gift from Dr. Jun-ichi Nakayama. K.A. was supported by JSPS KAKENHI grants (nos. 18H02444, 19H05798, and 22H02625). Y.G. was supported by a JST, ACT-X grant (no. JPMJAX22B8), by JSPS KAKENHI grants (nos. 19K16050 and 22K15110), by a Jigami Yoshifumi Memorial Research grant, and by a Sumitomo Research grant. K.S. was supported by a JSPS KAKENHI grant (no. 22J10844) and The Graduate University for Advanced Studies, SOKENDAI (SOKENDAI Student Dispatch Program). Y.K. was supported by a JSPS KAKENHI grant (no. 19H05675).

Author affiliations: [a]Quantitative Biology Research Group, Exploratory Research Center on Life and Living Systems, National Institutes of Natural Sciences, Myodaiji-cho, Okazaki, Aichi 444-8787, Japan; [b]Division of Quantitative Biology, National Institute for Basic Biology, National Institutes of Natural Sciences, Myodaiji-cho, Okazaki, Aichi 444-8787, Japan; [c]Department of Basic Biology, School of Life Science, SOKENDAI (The Graduate University for Advanced Studies), Myodaiji-cho, Okazaki, Aichi 444-8787, Japan; [d]Division of Integrated Life Science, Department of Gene Mechanisms, Laboratory of Cell Cycle Regulation, Graduate School of Biostudies, Kyoto University, Kyoto 606-8315, Japan; and [e]Center for Living Systems Information Science, Graduate School of Biostudies, Kyoto University, Kyoto 606-8315, Japan

Author contributions: K.S., Y.K., Y.G., and K.A. designed research; K.S. and Y.G. performed research; K.S. and Y.K. contributed new reagents/analytic tools; K.S. and Y.K. analyzed data; and K.S., Y.K., Y.G., and K.A. wrote the paper.

1. K. Luby-Phelps, D. L. Taylor, F. Lanni, Probing the structure of cytoplasm. *J. Cell Biol.* **102**, 2015–2022 (1986).
2. E. Moeendarbary *et al.*, The cytoplasm of living cells behaves as a poroelastic material. *Nat. Mater.* **12**, 253–261 (2013).
3. F. Etoc *et al.*, Non-specific interactions govern cytosolic diffusion of nanosized objects in mammalian cells. *Nat. Mater.* **17**, 740–746 (2018).
4. K. Nishizawa *et al.*, Universal glass-forming behavior of in vitro and living cytoplasm. *Sci. Rep.* **7**, 15143 (2017).

5. C. Di Rienzo, V. Piazza, E. Gratton, F. Beltram, F. Cardarelli, Probing short-range protein Brownian motion in the cytoplasm of living cells. *Nat. Commun.* **5**, 5891 (2014).
6. J. Xie *et al.*, Contribution of cytoplasm viscoelastic properties to mitotic spindle positioning. *Proc. Natl. Acad. Sci. U.S.A.* **119**, e2115593119 (2022).
7. M. C. Munder *et al.*, A pH-driven transition of the cytoplasm from a fluid- to a solid-like state promotes entry into dormancy. *Elife* **5**, e09347 (2016).
8. G. E. Neurohr, A. Amon, Relevance and regulation of cell density. *Trends Cell Biol.* **30**, 213–225 (2020).
9. M. Bonucci, T. Shu, L. J. Holt, How it feels in a cell. *Trends Cell Biol.* **33**, 924–938 (2023), 10.1016/j.tcb.2023.05.002.
10. A. T. Molines *et al.*, Physical properties of the cytoplasm modulate the rates of microtubule polymerization and depolymerization. *Dev. Cell* **57**, 466–479.e6 (2022).
11. B. Alric, C. Formosa-Dague, E. Dague, L. J. Holt, M. Delarue, Macromolecular crowding limits growth under pressure. *Nat. Phys.* **18**, 411–416 (2022).
12. M. Delarue *et al.*, mTORC1 controls phase separation and the biophysical properties of the cytoplasm by tuning crowding. *Cell* **174**, 338–349.e20 (2018).
13. K. Aoki, M. Yamada, K. Kunida, S. Yasuda, M. Matsuda, Processive phosphorylation of ERK MAP kinase in mammalian cells. *Proc. Natl. Acad. Sci. U.S.A.* **108**, 12675–12680 (2011).
14. D. Sang *et al.*, Condensed-phase signaling can expand kinase specificity and respond to macromolecular crowding. *Mol. Cell* **82**, 3693–3711.e10 (2022).
15. A. Miermont *et al.*, Severe osmotic compression triggers a slowdown of intracellular signaling, which can be explained by molecular crowding. *Proc. Natl. Acad. Sci. U.S.A.* **110**, 5725–5730 (2013).
16. A. Kitamura *et al.*, Increased intracellular crowding during hyperosmotic stress. *Sci. Rep.* **13**, 11834 (2023).
17. M. Guo *et al.*, Cell volume change through water efflux impacts cell stiffness and stem cell fate. *Proc. Natl. Acad. Sci. U.S.A.* **114**, E8618–E8627 (2017).
18. R. P. Joyner *et al.*, A glucose-starvation response regulates the diffusion of macromolecules. *Elife* **5**, e09376 (2016).
19. B. R. Parry *et al.*, The bacterial cytoplasm has glass-like properties and is fluidized by metabolic activity. *Cell* **156**, 183–194 (2014).
20. M. B. Heimlicher *et al.*, Reversible solidification of fission yeast cytoplasm after prolonged nutrient starvation. *J. Cell Sci.* **132**, jcs231688 (2019).
21. G. Marini, E. Nüske, W. Leng, S. Alberti, G. Pigino, Reorganization of budding yeast cytoplasm upon energy depletion. *Mol. Biol. Cell* **31**, 1232–1245 (2020).
22. C. R. Boyd-Shiwarski *et al.*, WNK kinases sense molecular crowding and rescue cell volume via phase separation. *Cell* **185**, 4488–4506.e20 (2022).
23. L. B. Persson, V. S. Ambati, O. Brandman, Cellular control of viscosity counters changes in temperature and energy availability. *Cell* **183**, 1572–1585.e16 (2020).
24. S. Plante, K.-M. Moon, P. Lemieux, L. J. Foster, C. R. Landry, Breaking spore dormancy in budding yeast transforms the cytoplasm and the solubility of the proteome. *PLoS Biol.* **21**, e3002042 (2023).
25. S. Ablett, A. H. Darke, P. J. Lillford, D. R. Martin, Glass formation and dormancy in bacterial spores. *Int. J. Food Sci. Technol.* **34**, 59–69 (1999).
26. A. E. Cowan, D. E. Koppel, B. Setlow, P. Setlow, A soluble protein is immobile in dormant spores of Bacillus subtilis but is mobile in germinated spores: Implications for spore dormancy. *Proc. Natl. Acad. Sci. U.S.A.* **100**, 4209–4214 (2003).
27. J. Dijksterhuis, J. Nijsse, F. A. Hoekstra, E. A. Golovina, High viscosity and anisotropy characterize the cytoplasm of fungal dormant stress-resistant spores. *Eukaryot. Cell* **6**, 157–170 (2007).
28. J. Buitink, O. Leprince, Glass formation in plant anhydrobiotes: Survival in the dry state. *Cryobiology* **48**, 215–228 (2004).
29. T. C. Boothby *et al.*, Tardigrades use intrinsically disordered proteins to survive desiccation. *Mol. Cell* **65**, 975–984.e5 (2017).
30. M. Sakurai *et al.*, Vitrification is essential for anhydrobiosis in an African chironomid, *Polypedilum vanderplanki*. *Proc. Natl. Acad. Sci. U. S. A.* **105**, 5093–5098 (2008).
31. D. Riveline, P. Nurse, "Injecting" yeast. *Nat. Methods* **6**, 513–514 (2009).
32. R. M. Garner, A. T. Molines, J. A. Theriot, F. Chang, Vast heterogeneity in cytoplasmic diffusion rates revealed by nanorheology and Doppelgänger simulations. *Biophys. J.* **122**, 767–783 (2023).
33. J. Lemière, F. Chang, Quantifying turgor pressure in budding and fission yeasts based upon osmotic properties. bioRxiv [Preprint] (2023). https://doi.org/10.1101/2023.06.07.544129 (Accessed 1 April 2024).
34. J. Lemière, P. Real-Calderon, L. J. Holt, T. G. Fai, F. Chang, Control of nuclear size by osmotic forces in Schizosaccharomyces pombe. *Elife* **11**, e76075 (2022).
35. M. Hatanaka, C. Shimoda, The cyclic AMP/PKA signal pathway is required for initiation of spore germination in Schizosaccharomyces pombe. *Yeast* **18**, 207–217 (2001).
36. H. Tsuyuzaki, R. Ujiie, M. Sato, Wake-up alarm: Virtual time-lapse gene expression landscape illuminates mechanisms underlying dormancy breaking of germinating spores. *Curr. Genet.* **67**, 519–534 (2021), 10.1007/s00294-021-01177-0.
37. D. Bonazzi *et al.*, Symmetry breaking in spore germination relies on an interplay between polar cap stability and spore wall mechanics. *Dev. Cell* **28**, 534–546 (2014).
38. C. Shimoda, Differential effect of glucose and fructose on spore germination in the fission yeast, Schizosaccharomyces pombe. *Can. J. Microbiol.* **26**, 741–745 (1980).
39. H. Tsuyuzaki *et al.*, Time-lapse single-cell transcriptomics reveals modulation of histone H3 for dormancy breaking in fission yeast. *Nat. Commun.* **11**, 1265 (2020).
40. W. Wei *et al.*, The Cdc42 GAP Rga6 promotes monopolar outgrowth of spores. *J. Cell Biol.* **222**, e202202064 (2023).
41. T. Maeda, Y. Watanabe, H. Kunitomo, M. Yamamoto, Cloning of the pka1 gene encoding the catalytic subunit of the cAMP-dependent protein kinase in Schizosaccharomyces pombe. *J. Biol. Chem.* **269**, 9632–9637 (1994).
42. G. Yu, J. Li, D. Young, The Schizosaccharomyces pombe pka1 gene, encoding a homolog of cAMP-dependent protein kinase. *Gene* **151**, 215–220 (1994).
43. C. S. Hoffman, Glucose sensing via the protein kinase A pathway in Schizosaccharomyces pombe. *Biochem. Soc. Trans.* **33**, 257–260 (2005).
44. C. Basier, P. Nurse, The cell cycle and cell size influence the rates of global cellular translation and transcription in fission yeast. *EMBO J.* **42**, e113333 (2023).
45. J. Atkin *et al.*, Torin1-mediated TOR kinase inhibition reduces Wee1 levels and advances mitotic commitment in fission yeast and HeLa cells. *J. Cell Sci.* **127**, 1346–1356 (2014).
46. M. Guo *et al.*, Probing the stochastic, motor-driven properties of the cytoplasm using force spectrum microscopy. *Cell* **158**, 822–832 (2014).
47. R. J. Pelham Jr., F. Chang, Role of actin polymerization and actin cables in actin-patch movement in Schizosaccharomyces pombe. *Nat. Cell Biol.* **3**, 235–244 (2001).
48. M. Minagawa, M. Shirato, M. Toya, M. Sato, Dual impact of a benzimidazole resistant β-tubulin on microtubule behavior in fission yeast. *Cells* **10**, 1042 (2021).
49. Y. Xie, T. Liu, D. Gresham, L. J. Holt, mRNA condensation fluidizes the cytoplasm. bioRxiv [Preprint] (2023). https://doi.org/10.1101/2023.05.30.542963 (Accessed 1 April 2024).
50. K. Takeda, C. Starzynski, A. Mori, M. Yanagida, The critical glucose concentration for respiration-independent proliferation of fission yeast, Schizosaccharomyces pombe. *Mitochondrion* **22**, 91–95 (2015).
51. M. Takaine, M. Ueno, K. Kitamura, H. Imamura, S. Yoshida, Reliable imaging of ATP in living budding and fission yeast. *J. Cell Sci.* **132**, jcs230649 (2019).
52. H. Inoue, C. Shimoda, Changes in trehalose content and trehalase activity during spore germination in fission yeast, Schizosaccharomyces pombe. *Arch. Microbiol.* **129**, 19–22 (1981).
53. F. F. Beltran, R. Castillo, J. Vicente-Soler, J. Cansado, M. Gacto, Role for trehalase during germination of spores in the fission yeast Schizosaccharomyces pombe. *FEMS Microbiol. Lett.* **193**, 117–121 (2000).
54. J. Cansado, T. Soto, J. Fernandez, J. Vicente-Soler, M. Gacto, Characterization of mutants devoid of neutral trehalase activity in the fission yeast Schizosaccharomyces pombe: Partial protection from heat shock and high-salt stress. *J. Bacteriol.* **180**, 1342–1345 (1998).
55. J. Mata, R. Lyne, G. Burns, J. Bähler, The transcriptional program of meiosis and sporulation in fission yeast. *Nat. Genet.* **32**, 143–147 (2002).
56. K. Luby-Phelps, P. E. Castle, D. L. Taylor, F. Lanni, Hindered diffusion of inert tracer particles in the cytoplasm of mouse 3T3 cells. *Proc. Natl. Acad. Sci. U.S.A.* **84**, 4910–4913 (1987).
57. K. Luby-Phelps, "Cytoarchitecture and physical properties of cytoplasm: Volume, viscosity, diffusion, intracellular surface area" in *International Review of Cytology*, H. Walter, D. E. Brooks, P. A. Srere, Eds. (Academic Press, 1999), pp. 189–221.
58. Y. Xie, D. Gresham, L. J. Holt, Increased mesoscale diffusivity in response to acute glucose starvation. *MicroPubl. Biol.* **2023**, 10.17912/micropub.biology.000729 (2023).
59. S. C. Weber, M. A. Thompson, W. E. Moerner, A. J. Spakowitz, J. A. Theriot, Analytical tools to distinguish the effects of localization error, confinement, and medium elasticity on the velocity autocorrelation function. *Biophys. J.* **102**, 2443–2450 (2012).
60. X. Shi *et al.*, Determination of dissociation constants in living zebrafish embryos with single wavelength fluorescence cross-correlation spectroscopy. *Biophys. J.* **97**, 678–686 (2009).
61. T. Sudhaharan *et al.*, Determination of in vivo dissociation constant, KD, of Cdc42-effector complexes in live mammalian cells using single wavelength fluorescence cross-correlation spectroscopy*. *J. Biol. Chem.* **284**, 13602–13609 (2009).
62. M. Kinjo, H. Sakata, S. Mikuni, Basic fluorescence correlation spectroscopy setup and measurement. *Cold Spring Harb. Protoc.* **2011**, 1262–1266 (2011).
63. L. Sigaut, J. E. Pearson, A. Colman-Lerner, S. Ponce Dawson, Messages do diffuse faster than messengers: Reconciling disparate estimates of the morphogen bicoid diffusion coefficient. *PLoS Comput. Biol.* **10**, e1003629 (2014).
64. T. Kühn *et al.*, Protein diffusion in mammalian cell cytoplasm. *PLoS One* **6**, e22962 (2011).
65. B. Pando, S. P. Dawson, D.-O.D. Mak, J. E. Pearson, Messages diffuse faster than messengers. *Proc. Natl. Acad. Sci. U.S.A.* **103**, 5338–5342 (2006).
66. M. A. Vibhute *et al.*, Transcription and translation in cytomimetic protocells perform most efficiently at distinct macromolecular crowding conditions. *ACS Synth. Biol.* **9**, 2797–2807 (2020).
67. Y. Chen, J.-H. Huang, C. Phong, J. E. Ferrell, Protein homeostasis from diffusion-dependent control of protein synthesis and degradation. bioRxiv [Preprint] (2023). https://doi.org/10.1101/2023.04.24.538146 (Accessed 1 April 2024).
68. N. K. Jain, I. Roy, Effect of trehalose on protein structure. *Protein Sci.* **18**, 24–36 (2009).
69. H. Tapia, D. E. Koshland, Trehalose is a versatile and long-lived chaperone for desiccation tolerance. *Curr. Biol.* **24**, 2758–2766 (2014).
70. S. X. Kim, G. Çamdere, X. Hu, D. Koshland, H. Tapia, Synergy between the small intrinsically disordered protein Hsp12 and trehalose sustain viability after severe desiccation. *Elife* **7**, e38337 (2018).
71. F. He *et al.*, Effect of sugar molecules on the viscosity of high concentration monoclonal antibody solutions. *Pharm. Res.* **28**, 1552–1560 (2011).
72. L. Dengler, M. Örd, L. M. Schwab, M. Loog, J. C. Ewald, Regulation of trehalase activity by multi-site phosphorylation and 14-3-3 interaction. *Sci. Rep.* **11**, 962 (2021).
73. T. Soto, J. Fernandez, J. Cansado, J. Vicente-Soler, M. Gacto, Glucose-induced, cyclic-AMP-independent signalling pathway for activation of neutral trehalase in the fission yeast Schizosaccharomyces pombe. *Microbiology* **141**, 2665–2671 (1995).
74. A. Franco *et al.*, Functional characterization of Schizosaccharomyces pombe neutral trehalase altered in phosphorylatable serine residues. *Arch. Microbiol.* **183**, 394–400 (2005).
75. D. Carrillo, J. Vicente-Soler, M. Gacto, Cyclic AMP signalling pathway and trehalase activation in the fission yeast Schizosaccharomyces pombe. *Microbiology* **140**, 1467–1472 (1994).
76. N. Bellotto *et al.*, Dependence of diffusion in Escherichia coli cytoplasm on protein size, environmental conditions, and cell growth. *Elife* **11**, e82654 (2022).
77. K. Nishizawa *et al.*, Feedback-tracking microrheology in living cells. *Sci. Adv.* **3**, e1700318 (2017).
78. K. Sakai, Y. Kondo, Y. Goto, K. Aoki, Dataset for "Cytoplasmic fluidization contributes to breaking spore dormancy in fission yeast." SSBD. https://ssbd.riken.jp/repository/360/. Deposited 5 June 2024.